Journal of Materials Chemistry A

Accepted Manuscript

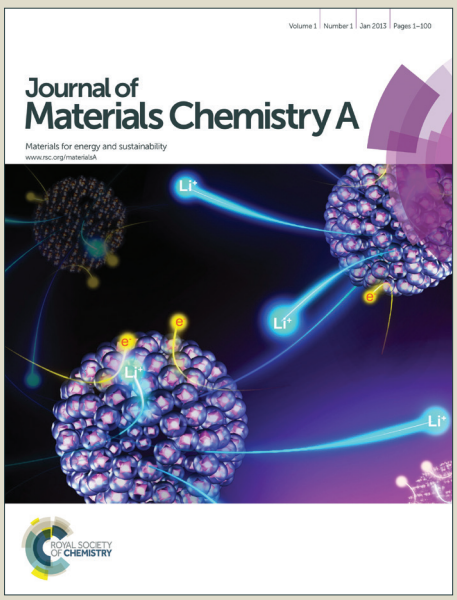

ROYAL SOCIETY OF CHEMISTRY

www.rsc.org/materialsA

Journal of Materials Chemistry A

Journal of Materials Chemistry A

Dynamic Article Links ►

Cite this: DOI: 10.1039/c0xx00000x

www.rsc.org/xxxxxx

PAPER

Ultra-low gas permeability and efficient reinforcement of cellulose nanocomposite films by well aligned graphene oxide nanosheets†

Hua-Dong Huang,[a] Chun-Yan Liu,[a] Dan Li,[a] Yan-Hui Chen,[b] Gan-Ji Zhong,*[a] Zhong-Ming Li*[a]

Received (in XXX, XXX) Xth XXXXXXXXX 20XX, Accepted Xth XXXXXXXXX 20XX

DOI: 10.1039/b000000x

Cellulose is well considered as an ideal green candidate for biodegradable packaging films, but the insufficient gas barrier performance is its weakness. In the current study, a simple, efficient, low cost, recyclable, non-toxic and environmentally friendly green processing solvent, sodium hydroxide (NaOH)/urea aqueous solution, was utilized to fabricate graphene oxide nanosheet (GONS)/regenerated cellulose nanocomposite films with ultra-low O_2 permeability and high mechanical performances. Transmission electrical microscope and two-dimensional wide angle X-ray diffraction measurements showed that GONSs were fully exfoliated, homogeneously dispersed and highly aligned along the surface of cellulose nanocomposite films. Rheological and fourier-transform infrared spectroscopy measurements demonstrated the existence of strong H-bonding interactions between GONSs and cellulose matrix. A significant improvement on barrier properties of the regenerated cellulose nanocomposite films was achieved. O_2 permeability coefficient was reduced by about 1000 times relative to the neat regenerated cellulose film at a rather low GONS loading of 1.64 vol%. Tensile strength and Young's modulus of the regenerated cellulose nanocomposite films were enhanced by about 67% and 68% compared to RC film, respectively. The theoretical simulation results of Cussler and Halpin-Tsai models consistently confirmed that GONSs were apt to align parallel to the film surface, which was probably induced by gravitational forces and was further consolidated by hot pressing. The work presented here indicates that such a simple and environmentally friendly method is an effective strategy to design highly aligned nanofillers in polymer nanocomposite films and the obtained cellulose nanocomposite films have an excellent potential as packaging materials for protecting susceptible to O_2 degradation of perishable goods.

1. Introduction

Nowadays, polymer films are in great demand in many packaging and protective applications, such as food industry, pharmaceuticals, and electronic devices, owing to their lightweight, versatile, inexpensive and easily processing features. Nevertheless, most commonly used polymer films are produced from fossil fuels, discarded as burnable wastes or used as landfills after their useful life, thus, causing an overdependence on the limited petroleum resources and a serious environmental pollution. As such, it is of high significance to develop more environmentally friendly alternatives in the packaging applications with the rapidly growing awareness of sustainability in the recent years.[1,2] Cellulose, the most affluent natural polysaccharide on the planet, is increasingly receiving burgeoning research interest as a promising candidate to substitute for petrochemical-based polymers in many cases including packaging applications due to its low-cost, renewable, biodegradable, and biocompatible features.[3,4] However, the intransigent molecular structure of native cellulose with large proportion of strong intra- and inter-molecular hydrogen bonding makes it difficult to process native cellulose in common solvents or as a melt. The presence of special solvent systems (ionic liquids,[5-7] *N*-methylmorpholine-*N*-oxide hydrate,[8] *N, N*-dimethylacetamide/LiCl,[9,10] and aqueous alkali/urea,[11-14] *etc.*) opens up a new avenue to directly dissolve cellulose for preparing packaging films. Unfortunately, as a packaging material, the regenerated cellulose film exhibits insufficient oxygen barrier performances for various oxygen-sensitive commodities, especially at high humidity, which is viewed as a stumbling block to restrict the development and application of the regenerated cellulose in the packaging and protective industry.

Incorporation of nanoplatelets into polymer has been developed over the past decades as an alternative strategy to fabricate high barrier polymer films.[15-24] In this scenario, the nanoplatelets act as multiple physical barriers to diffusing molecules, significantly enhancing the barrier properties of polymer-based nanocomposites. The enhancement efficiency strongly depends on the nanoplatelets' morphology (*i.e.*, exfoliation, dispersion, and orientation) in the polymer matrix, their intrinsic properties (high surface areas, high aspect ratios, *etc.*), as well as on the interfacial adhesion between nanoplatelets and polymer matrix. In particular, the highly aligned nanoplatelets perpendicular to diffusion direction can maximumly increase the tortuosity of penetration path for diffusing molecules. Hitherto, as

representative plate-like nanofillers, the impermeable layered nanoclays are proverbially used to heighten barrier performances of many polymeric films, including polyethylene,[19] poly(vinyl alcohol),[20] poly(lactic acid),[21] polyurethane,[22] or even native cellulose films[23] and regenerated cellulose ones,[24] *etc*. However, when employing conventional processing techniques, it still remains a great challenging issue to obtain completely exfoliated and highly aligned nanoclays. As a result, the intercalated or aggregated morphology is typically shown in the nanocomposites, causing only modest improvement on their gas barrier performances.

Recently, geometrically analogous to nanoclays, graphene oxide nanosheets (GONSs) have sparked great excitement in carbon-based nanocomposites as highly effective barrier performance enhancers due to their tightly packed planar structure, extremely high specific surface areas and large aspect ratios.[25-34] More interestingly, a cornucopia of oxygen-containing functional groups in the form of hydroxyl, epoxide, carbonyl and carboxyl endow GONSs with excellent hydrophility, rendering GONSs easily exfoliated into individual nanosheets and evenly dispersed in a polar polymer matrix. Consequently, the interfacial adhesion is improved significantly. Hence, GONSs are promising alternative candidates to develop high barrier polar polymer-based nanocomposite films. For instance, a ground-breaking achievement has been obtained by Grunlan *et al*. *via* layer-by-layer assembly to fabricate GONS/branched polyethylenimine multilayer thin films, revealing super gas barrier performance with an O_2 permeability coefficient of 2.5×10^{-20} cm^3 cm cm^{-2} s^{-1} Pa^{-1}, which was comparable to a 100 nm SiO_x nanocoating and two orders of magnitude better than a 25 μm ethylene-vinyl alcohol copolymer film.[28] The water-vapor-transmission-rate of polyimide nanocomposite films was significantly reduced by about 83% from 181 to 30 g mil m^{-2} day^{-1} with the addition of only 0.01 wt% GONSs.[29] In our previous work, a simple and environmentally friendly method was proposed to prepare high barrier GONS/poly(vinyl alcohol) nanocomposite films, wherein about 98% and 68% decline in O_2 and water vapor permeability coefficients was achieved at a rather low GONS loading of 0.72 vol%.[30] The basis of these studies motives us to harness the fascinating barrier properties of GONSs for effectively boosting up the gas barrier properties of regenerated cellulose films in consideration of the polar hydroxyl groups on its molecular chain. Yet, as far as we know, very few efforts have been devoted to improve the barrier performance regenerated cellulose films by GONSs.

Taking these considerations into account, in the current study, a simple, efficient, low cost, recyclable, non-toxic and environmentally friendly green processing solvent, sodium hydroxide (NaOH)/urea aqueous solution,[35] was utilized to prepare GONS/regenerated cellulose nanocomposite films. The obtained nanocomposite films showed ultra-low gas permeability with an O_2 permeability coefficient of 0.01×10^{-14} cm^3 cm cm^{-2} s^{-1} Pa^{-1}, which was about 1000 times lower than that of the neat regenerated cellulose film. Simultaneously, mechanical properties of the cellulose nanocomposite films were enhanced by a large margin at a rather low GONS loading. These results were attributed to the fully exfoliation, uniform dispersion and horizontal alignment of GONSs, as well as strong interfacial adhesion between GONSs and regenerated cellulose matrix.

2. Experimental Section

2.1. Materials

Cellulose sample (cotton linters, with a degree of polymerization of about 500 ± 50) was supplied by Hubei Jinhuan *Co*., *Ltd*. (Xiangfan, China). It was vacuum-dried at 60 °C for 24 h to remove any moisture before use. GONSs were prepared by the modified "Hummers" method from expandable graphite with an expansion rate of 200 ml g^{-1}, which was purchased from Qingdao Haida Graphite *Co*., *Ltd*., China. Details of preparation process were reported in our previous work.[36] NaOH and urea were purchased from Chengdu Kelong Chemical Reagent Factory, Chengdu, China. Unless otherwise stated, all other reagents were of analytical grade and directly used as received without further purification.

2.2. Preparation of GONS/Regenerated Cellulose Nanocomposite Films

A solution of NaOH/urea/H_2O with a weight ratio of 7:12:81 was utilized as the processing solvent to prepare a series of the regenerated cellulose nanocomposites containing various GONS loadings of 0.2, 0.5, 1.0, and 2.0 wt%. Taking the 0.2 wt% GONS as an example, the detailed procedures were as follows: 5 mg of graphite oxide obtained by modified "Hummers" method was initially dispersed into a given amount of distilled water with vigorous agitation and ultrasonic treatment for 60 min at room temperature. In this process, graphite oxide was completely exfoliated into individual nanosheets, forming a stable and uniform suspension. The designed amount of NaOH and urea were directly dissolved into the GONS suspension and the mixture was precooled to -12.0 ^{o}C. Subsequently, 2.5 g cellulose was immediately added into the mixture with strong stirring at 3000 rpm for 5 min at the ambient temperature to obtain transparent GONS/cellulose solution, wherein the concentration of cellulose is kept constant at 2.5 wt%. The resultant homogeneous dispersion was degassed by a circulating bath vacuum pump for 1 h at 0 ^{o}C, cast into a glass holder at room temperature for 12 h to allow gelation, and immersed in distilled water bath at room temperature to remove NaOH and urea. The washing distilled water was replaced regularly with fresh water several times until there were no salts. Finally, in order to avoid wrinkling, the wet GONS/regenerated film was dried under a certain pressure at 150 ^{o}C for 10 min until its weight equilibrated to obtain a nanocomposite film with the thickness of about 90 μm (Fig. S1, ESI†). The weight content of GONSs in the nanocomposites was converted to volume content using the density of cellulose matrix and GONSs, 1.5 and 1.8 g cm^{-3}, respectively. Thus, the volume content of GONSs incorporated into GONS/regenerated cellulose nanocomposite film can be considered as 0.17, 0.41, 0.83, and 1.64 vol%, which were coded as RC0.17, RC0.41, RC0.83, and RC1.64. And for comparison, neat regenerated cellulose film was prepared according to the same procedures, which could be abbreviated as RC.

2.3. Dispersion Morphology of GONSs in regenerated cellulose matrix

GONS morphology was observed by a field emission scanning

electron microscope (SEM) (FEI Inspect-F, Finland) with an acceleration voltage of 5 kV to characterize the cross sections of the films. The samples (RC and RC1.64) for SEM images were cryo-fractured in liquid nitrogen and then coated with a thin layer of gold prior to being observed. Cross section of cellulose nanocomposite film was further imaged via using a FEI Tecnai F20 transmission electron microscope (TEM) at an acceleration voltage of 200 kV. The sample was prepared for imaging by embedding a piece of nanocomposite film at a GONS loading of 1.64 vol% in epoxy and a thin section was obtained with a microtome equipped with a diamond knife.

2.4. Two-Dimensional Wide Angle X-ray Diffraction (2D-WAXD) Characterization

2D-WAXD patterns were collected at the Advanced Polymers Beamline (X27C, λ = 0.1371 nm) in the National Synchrotron Light Source (NSLS), Brookhaven National Laboratory (BNL). An MAR CCD detector (MAR-USA) with a resolution of 1024 × 1024 pixels (pixel size = 158 μm) was used to acquire data for wide-angle experiments. An aluminum oxide standard was used to calibrate the scattering angle, and the background of air scattering was subtracted. The distance between the sample and detector was 132.6 mm. WAXD profiles were obtained from circularly integrated intensities of the 2D-WAXD patterns. The crystallinity (χ_c) of all samples obtained by a standard peak-fit procedure can be estimated by the following equation:

$$\chi_c = \frac{\sum A_{\text{cryst}}}{\sum A_{\text{cryst}} + \sum A_{\text{amorp}}} \times 100\% \quad (1)$$

where $\sum A_{\text{cryst}}$ and $\sum A_{\text{amorp}}$ are the fitted areas of the crystal and amorphous phases, respectively.

2.5. Rheological Measurement

The effect of GONSs on the gelation process of cellulose in the NaOH/urea aqueous solution was investigated by a MAR III dynamic rheometer (Thermo Fisher Scientific, USA) equipped with a couple of parallel plates. The diameter of plates was 35 mm and the measurement gap between the plates was 2 mm. The value of the stain amplitude was fixed at 5%, which is within a linear viscoelastic region and the sweep of frequency was set at 1 Hz. The storage modulus (G') and loss modulus (G'') were detected as a function of temperature from 15 to 80 ^{o}C at a heating rate of 2 ^{o}C/min.

2.6. Fourier-Transform Infrared Spectroscopy (FTIR) Characterization

FTIR characterization was performed on a Nicolet 6700 spectrometer (Thermo Fisher Scientific, USA) in reflection-transmission mode. The spectra were collected over the wavenumber range of 4000-700 cm^{-1} by averaging 32 scans with the resolution of 2 cm^{-1}, which has already been subtracted from the background spectra.

2.7. Mechanical Testing

According to ASTM standard D638, the mechanical properties of cellulose nanocomposite films were determined on a universal tensile instrument (Model 5576, Instron Instrument, USA) with a span length of 20 mm at a testing speed of 1.0 mm/min. Before testing, the cellulose films were tailored into rectangular strips with the same width of about 10 mm, and thickness was separately measured for each sample. The average values and standard deviations of mechanical properties were evaluated for at least five samples.

2.8. Barrier Testing

O_2 permeation analysis of cellulose nanocomposite films was conducted under constant volume-variable pressure conditions using a VAC-V_2 film permeability testing machine (labthink instruments, Jinan, China) at room temperature with 50% relative humidity according to ISO2556:1974. The gas permeation cell was separated into two compartments by film samples with 100 mm in diameter. The feed pressure was 1 atm of O_2 and the permeate pressure as a function of time were recorded by pressure sensors to calculate the gas permeability coefficient. In our study, regenerated cellulose films were a bit too brittle for O_2 permeation measurement and they all fractured during the experiments. Thus, all the regenerated cellulose nanocomposites films were toughened with glycerol[37] and the resultant films could be successfully subjected to barrier measurements. The average content of glycerol in the toughened films was about 14.8 wt% (Table S1, ESI†).

3. Results and Discussion

3.1 Dispersion of individual GONSs in the cellulose nanocomposite films

The dispersion of GONSs in the preparation process of cellulose nanocomposite films includes three stages (Fig. S2, ESI†). GONSs are initially dispersed in water in the form of uniform colloids (Fig. S2a, ESI†), but they seriously aggregate in the aqueous solution of NaOH/urea (Fig. S2b, ESI†). Fortunately, the presence of cellulose molecules effectively prevents the aggregation of GONSs, forming a homogeneous suspension of cellulose and GONSs (Fig. S2c, ESI†). This may be indicative of the existence of strong intermolecular interactions between GONSs and cellulose molecules.

The resultant regenerated cellulose films were observed by SEM and TEM to further evaluate the GONS dispersion. Fig. 1a and b show the SEM images of the fracture surfaces of regenerated cellulose films. Both RC and RC1.64 display a dense and homogeneous texture, and no any trace of GONSs is visible in RC1.64. Such architecture indirectly suggests efficient dispersion of GONSs, possibly due to strong interfacial adhesion that stabilizes individual GONS dispersion. Fig. 1c and d present the typical TEM images of RC1.64. It is vivid that GONSs are fully exfoliated into individual nanosheets with a thickness of about 1.5 nm and homogeneously dispersed in the cellulose matrix. More interestingly, as shown in Fig. 1c, GONSs are inclined to highly align to the surface of cellulose nanocomposite film. Such perfect orientation and uniform dispersion of GONSs allow to expect enhanced performance of cellulose[30,38].

Cite this: DOI: 10.1039/c0xx00000x

www.rsc.org/xxxxxx

PAPER

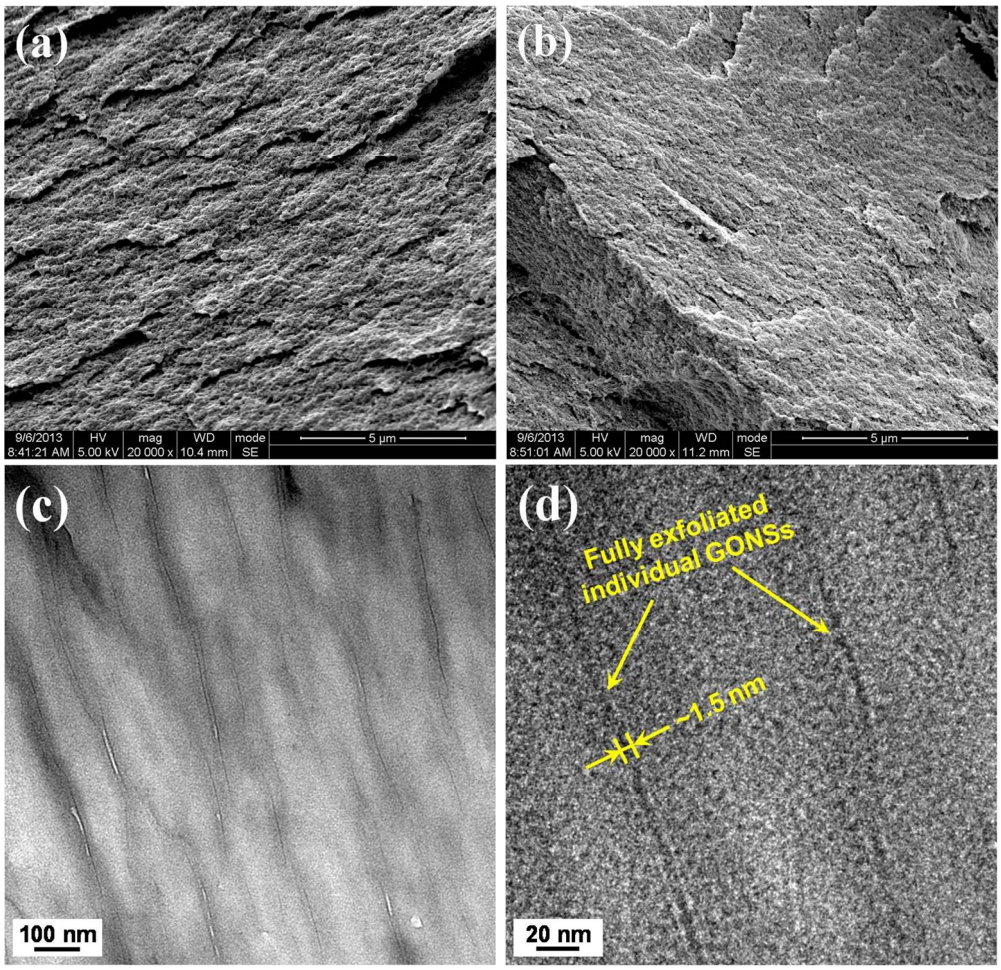

Fig. 1 Typical SEM images for the fractured surface of RC (a) and RC1.64 (b), and TEM images of RC1.64 with (c) low- and (d) high-magnification.

The dispersion of individual GONSs in the cellulose matrix is further determined by the interlayer spacing changes of GONSs using 2D-WAXD measurement. Fig. 2 illustrates the representative 2D-WAXD patterns of graphite oxide, RC and cellulose nanocomposite samples. The characteristic diffraction ring of GONSs is absent in the cellulose nanocomposite, signifying that the regular and periodic structure of graphite oxide disappears. It can be seen more vividly in Fig. 3 that a typical (002) reflection of graphite oxide is observed at 2θ = 9.8°, corresponding to a layer-to-layer distance of 0.80 nm. It is significantly larger than that of pristine graphite (~0.34 nm), arising from the presence of covalently bound oxygen-containing functional groups and the amount of absorbed water.[39] We can also notice that the cellulose nanocomposite samples have only two same distinct diffraction peaks at 17.8° and 19.2° as that of RC with no diffraction peak of graphite oxide. This result adequately confirms that completely exfoliated and uniformly dispersed GONSs are achieved in the cellulose matrix, yielding the consistent results with TEM observation. Additionally, as shown in Fig. 2, the two homogeneous diffraction rings of RC and cellulose nanocomposite samples suggest that cellulose crystals are isotropically distributed in the regenerated cellulose films and the addition of GONSs has no impact on the crystalline modification of cellulose. The representative crystalline structure of regenerated cellulose is assigned to crystalline form of cellulose II, which generally originates from the polymorphic transformation of cellulose I by alkali treatment (Fig. S3, ESI†).[40,41] Besides, the χ_c in the cellulose nanocomposite films determined by Equation (1), is quasi-identical to that of RC film (~ 50%), slightly varying in the range of 48% ~ 53%.

Journal of Materials Chemistry A

Cite this: DOI: 10.1039/c0xx00000x

www.rsc.org/xxxxxx

PAPER

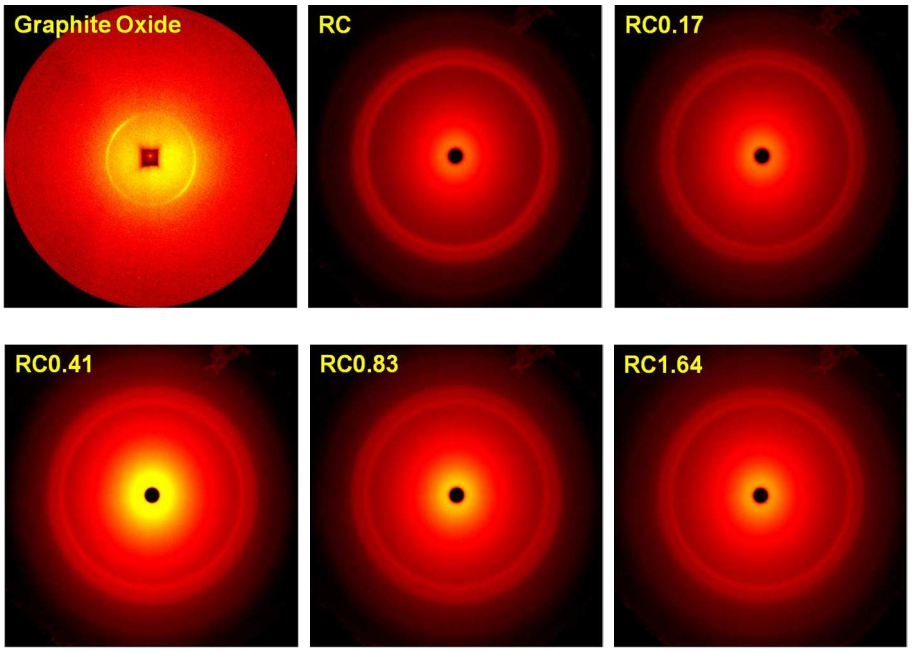

Fig. 2 2D-WAXD patterns of graphite oxide, RC, and cellulose nanocomposite samples as a function of GONS loadings.

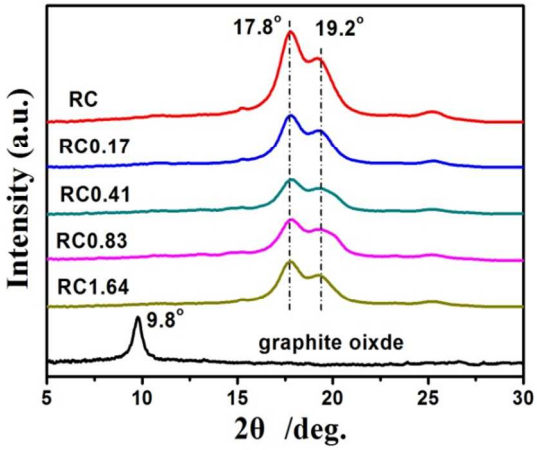

Fig. 3 1D-WAXD intensity profiles of graphite oxide, RC, and cellulose nanocomposite samples as a function of GONS loadings, integrated circularly from their corresponding 2D-WAXD patterns in Fig. 2.

3.2. Interfacial adhesion between GONSs and cellulose

It is well established that not only the dispersion of GONSs, but also the interfacial interactions between GONSs and polymer matrix play a crucial role in the successful development of high-performance GONS-based nanocomposites. Herein, rheological and FTIR measurements are carried out to investigate the interactions between GONSs and cellulose chains. As a rule of thumb, the stability of cellulose solution in the NaOH/urea aqueous solvent is greatly dependent on temperature.[42] Upon heating, the hydrogen bonding between cellulose and solvent is gradually broken to expose the hydroxyl groups of cellulose to each other, giving a chance to regenerate the intra- and intermolecular hydrogen bonding of cellulose. As a consequence, the rheological behavior of cellulose solution changes significantly, accompanied by a thermal-induced irreversible sol-gel transition of cellulose. The crossover of storage modulus (G') and loss modulus (G'') curves is defined as the gel point.[43,44] Fig. 4 shows the temperature dependence of G' and G'' for RC and RC1.64 solutions at a heating rate of 2 °C/min. As the temperature rises, both G' and G'' values of RC solution increase, meaning the gelation temperature at 59.0 °C. When GONSs are incorporated, the sol-gel transition takes place earlier, displaying the gelation temperature at 51.6 °C. The origin of the advanced gelation temperature for cellulose nanocomposite solution can be interpreted by the hydrogen bonding interactions between the oxygen-containing functional groups on the basal plane and edges of GONSs and the hydroxyl groups on the cellulose molecular chains.[44-46] Besides, GONSs with extremely high specific surface area can effectively provide a large number of additional physically cross-linking points and brilliantly play a bridging role, promoting the self-association of cellulose chains and the formation of the gel network. The conclusion is further confirmed by the FTIR results as presented in Fig. 5. It is well known that the characteristic hydroxyl stretching band at 3650~3000 cm^{-1} is sensitive to hydrogen bonding,[30] which shifts to a lower wavenumber from 3329 to 3309 cm^{-1} at a GONS loading of 1.64 vol%. The band shift clearly demonstrates the presence of strong hydrogen bonding between GONSs and cellulose matrix, consequently dissociating the hydrogen bonding among the

hydroxyl groups in the cellulose chains. Such strong interfacial adhesion is beneficial in transferring the charming properties of GONSs to cellulose matrix through the interfacial region, so as to effectively achieve the high-performance of cellulose.

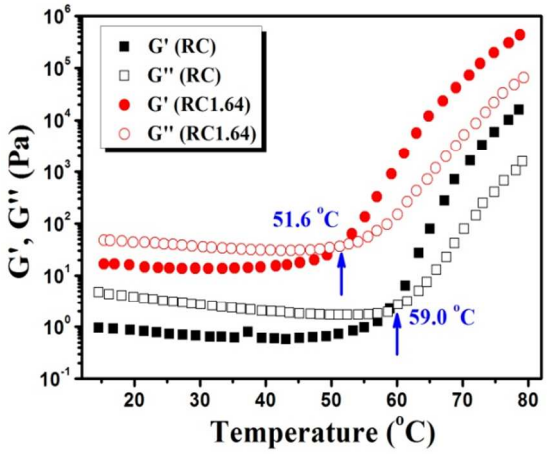

Fig. 4 Dependence of the storage and loss modulus of RC and RC1.64 solutions in the NaOH/urea aqueous solvent system on the elevated temperature at a heating rate of 2 °C/min.

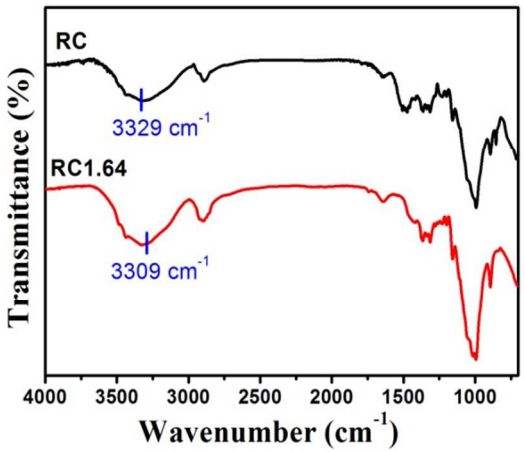

Fig. 5 FTIR spectra of RC and RC1.64 films over the wavenumber range of 4000-700 cm^{-1} with the resolution of 2 cm^{-1}.

3.3. Barrier Properties of RC and the cellulose nanocomposite films

Fig. 6 depicts permeability coefficient of O_2 (P_{O_2}) for RC and cellulose nanocomposite films as a function of GONS loadings. Upon the GONS loading, it is envisioned that a dramatic improvement on P_{O_2} of cellulose nanocomposite films is achieved, effectively suppressing the O_2 penetration in the cellulose nanocomposite films. To be specific, P_{O_2} of RC0.17 film is as low as 1.88×10^{-14} cm^3 cm cm^{-2} s^{-1} Pa^{-1}, which is almost 10 times lower than that of RC film (10.25×10^{-14} cm^3 cm cm^{-2} s^{-1} Pa^{-1}). Significantly, a further steady decrease in P_{O_2} is observed with increasing GONS loading from 0.17 to 0.83 vol%. The RC0.83 film exhibits P_{O2} of 0.16×10^{-14} cm^3 cm cm^{-2} s^{-1} Pa^{-1}, about 91% and 98% reduction relative to RC0.17 and RC films, respectively. As the GONS content further rises to 1.64 vol%, it is striking that a more than 1000 times decline in P_{O_2} from 10.25 $\times 10^{-14}$ to 0.01×10^{-14} cm^3 cm cm^{-2} s^{-1} Pa^{-1} is achieved. The value of O_2 permeability at 50% relative humidity for RC1.64 is much lower than that of high density polyethylene or poly(ethylene terephthalate), and is comparable to the practical petroleum-based O_2 barrier films such as poly(vinylidene chloride) usually used in packaging industry for food storage.[47] To the best of our knowledge, the remarkable enhancement on O_2 barrier properties of cellulose nanocomposite films with such a low GONS loading is unprecedented, which certifies that the cellulose nanocomposite films have the excellent potential as packaging materials for protecting susceptible to O_2 degradation of perishable goods.

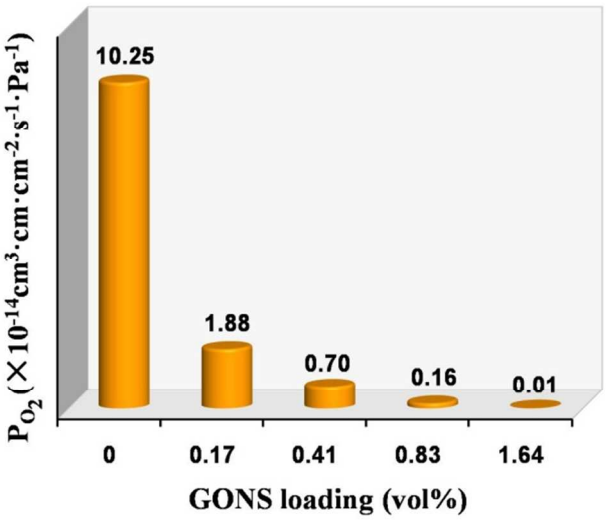

Fig. 6 Permeability coefficient of O_2 (P_{O_2}) for RC and cellulose nanocomposite films as a function of GONS loadings.

It is well accepted that the gas permeability of semi-crystalline polymer incorporated with nanoplatelets is greatly determined by the impermeable nanoplatelets, as well as its crystallinity and crystalline structure.[48-50] As depicted in Figs. 2 and 3, the cellulose crystals of all samples exhibit the same crystalline form (cellulose II), whose crystallinity falls into a very limited range between 48% and 53%. Therefore, it goes without saying that the ultra-low O_2 permeability is overwhelmingly ascribed to the addition of GONSs.

To further quantitatively analyze the impact of GONSs on the barrier properties of the cellulose nanocomposite films, experimental data are summarized in Fig. 7 as a plot of relative permeability (R_p) versus the volume content of GONSs. R_p is defined as follows:

$$R_p = \frac{P_c}{P_m} \quad (2)$$

where P_m and P_c are O_2 permeability coefficients of RC and cellulose nanocomposite films, respectively. The well-established Cussler model is often used to comparatively study the barrier performance of polymer nanocomposites[51] and its predicted values for R_p in terms of level of GONS loadings are shown in Fig. 7. In the Cussler model, the fully exfoliated and well dispersed nanoplatelets are assumed to be highly aligned throughout the entire polymer matrix. The corresponding R_p can be given by

$$R_p = \left(1 + \frac{\alpha_g^2 \varphi_g^2}{1 - \varphi_g}\right) \quad (3)$$

where α_g is the aspect ratio of GONSs, which was roughly estimated to be about 800 by TEM images (Fig. 1c). φ_g is the volume fraction of GONSs in the cellulose matrix. As illustrated in Fig. 7, it is worth noting that our experimental data about the decrease in R_p substantially mirror the Cussler prediction. Such good agreement suggests that GONSs in the cellulose have the morphology analogous to that described in the Cussler model; that is to say, GONSs are apt to align parallel to the film surface. This prediction is in well line with the observed morphology of GONSs in the cellulose (Fig. 1c). As described above, two aspects are responsible for the high barrier effectiveness of GONSs. Firstly, the impermeable GONSs are recognized as "nano-barrier wall", giving rise to the decrease in available area for diffusion and the increase in the tortuous pathway for diffusing molecules. The full exfoliation and uniform dispersion, especially for high orientation of GONSs in the cellulose can dramatically intensify the tortuosity of penetration paths for diffusing molecules. Moreover, the strong interfacial adhesion between GONSs and cellulose (Figs. 4 and 5) may restrict the mobility of cellulose chains and densify the interfacial region, subsequently providing less available free volume for diffusing molecules and leading to an increase in residence time of O_2 in the cellulose nanocomposite films.

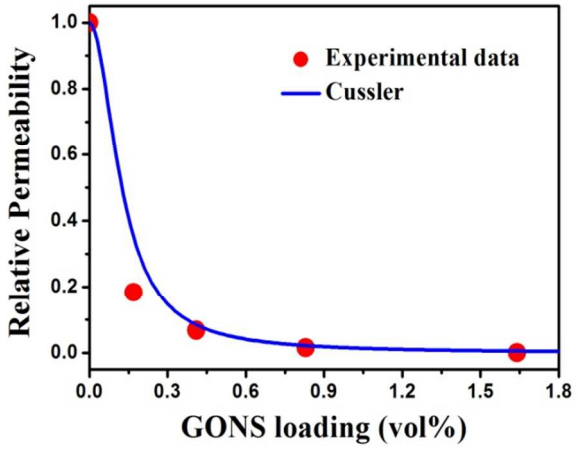

Fig. 7 Comparison between experimental data about P_{O_2} and Cussler model for the relative permeability R_p in terms of level of GONS loadings.

3.4. Mechanical Properties of RC and the cellulose nanocomposite films

The typical stress-strain curves of RC and the cellulose nanocomposite films are illustrated in Fig. 8. All cellulose samples with and without GONSs represent a normal brittle fracture behavior with less than 4% elongation at break.[45,46,52] The tensile strength and Young's modulus are shown in Fig. 9. The RC film possesses minimum tensile strength and Young's modulus, with the values of 50.1 MPa and 3.8 GPa, respectively. Addition of only 0.17 vol% leads to limited enhancement in mechanical properties of the cellulose nanocomposite films. However, as the GONS content rises up to 0.83 vol%, a substantial improvement in mechanical properties of GCN films is achieved, where the tensile strength and Young's modulus reach 68.0 MPa and 5.6 GPa, respectively. More significantly, the incorporation of 1.64 vol% GONSs maximumly heightens the tensile strength and Young's modulus to 83.5 MPa and 6.4 GPa, corresponding to the increases by 67% and 68% relative to RC film. Hitherto, graphene-based materials have been fabricated extensively to boost up the mechanical performances of regenerated cellulose using ionic liquids, *N*-methylmorpholine-*N*-oxide hydrate, *N, N*-dimethylacetamide/LiCl, and aqueous alkali/urea, etc. as a processing solvent.[45,46,52-54] The correspondingly enhanced mechanical properties are summarized in Table S2, ESI†, wherein it is clearly seen that the reinforcement efficiency of GONSs in this work is very attractive compared to other regenerated cellulose systems albeit limited available data.

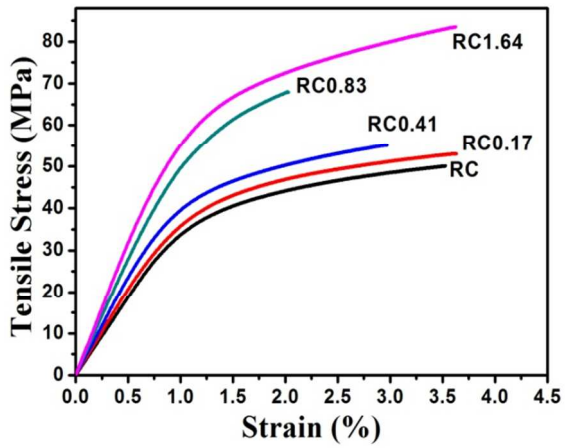

Fig. 8 Typical stress-strain curves of RC and cellulose nanocomposite films with different GONS loadings.

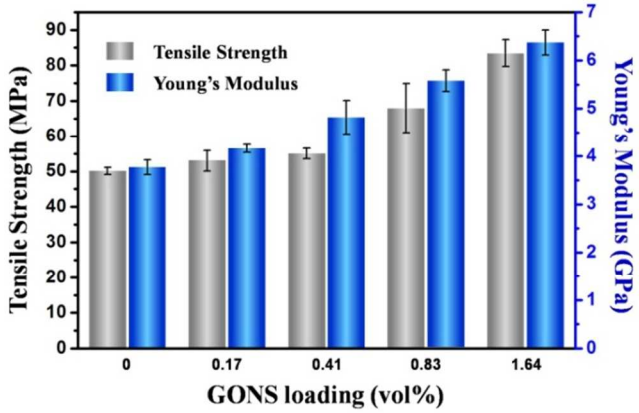

Fig. 9 Tensile strength and Young's modulus of RC and the cellulose nanocomposite films as a function of GONS loadings.

The well-established Halpin-Tsai model has been widely utilized to predict the modulus of randomly or unidirectionally distributed nanofiller-reinforced nanocomposites.[38,55,56] We attempt to use this model to unveil the mechanism of enhanced mechanical performance by GONSs/cellulose nanocomposite films. The Young's modulus of the cellulose nanocomposite films with randomly oriented (E_r) and unidirectionally distributed (E_u) GONSs can be calculated by the following equations:

$$E_r = E_m\left[\frac{3}{8}\frac{1+\eta_L\xi\varphi_g}{1-\eta_L\varphi_g}+\frac{5}{8}\frac{1+2\eta_T\varphi_g}{1-\eta_T\varphi_g}\right] \quad (4)$$

$$E_u = E_m\left[\frac{1+\eta_L\xi\varphi_g}{1-\eta_L\varphi_g}\right] \quad (5)$$

$$\eta_L = \frac{(E_g/E_m)-1}{(E_g/E_m)+\xi} \quad (6)$$

$$\eta_T = \frac{(E_g/E_m)-1}{(E_g/E_m)+2} \quad (7)$$

$$\xi = 2\alpha_g/3 \quad (8)$$

where α_g refers to the aspect ratio of GONSs and its value is the same as that used in the Cussler model (Fig. 7). E_m and E_g are the Young's modulus of RC film and GONSs, respectively. The Young's modulus of RC films is measured as 3.8 GPa from the experimental data. And the value of 207.6 GPa is used as the Young's modulus of GONSs, which is previously measured by Ruoff et al. through atomic force microscopy measurement combined with finite element method.[57] As shown in Fig. 10, it is visible that our experimentally measured Young's modulus is very close to the theoretical predictions under the assumption that GONSs are horizontally aligned along the surface of the cellulose nanocomposite films. This result is accordance with the theoretical simulation results of Cussler model (Fig. 9) and TEM results (Fig. 1c). Additionally, it is well accepted that mechanical performances of semi-polymer strongly depend on its crystalline structure and crystallinity.[58,59] As illustrated in Figs. 2 and 3, all the cellulose samples with the crystallinity of ~50% possess the same crystalline structure of cellulose II. Therefore, we can reasonably declare that the efficient reinforcement of the cellulose nanocomposite films are attributed to the fully exfoliated, uniformly dispersed, and horizontally aligned GONSs, as well as the strong interfacial adhesion between GONSs and cellulose matrix (Figs. 4 and 5), which can effectively facilitate the interfacial stress transfer.

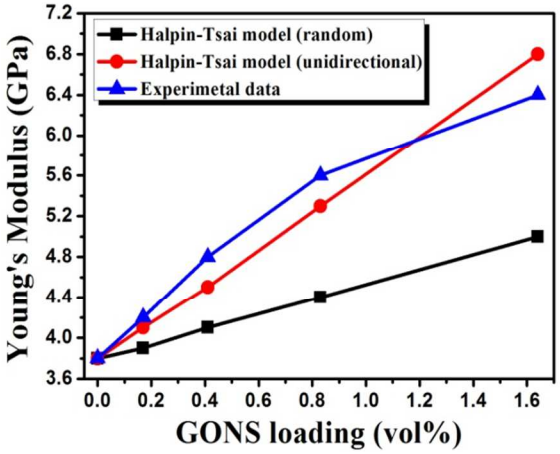

Fig. 10 Young's modulus of experimental samples and the theoretical values by Halpin-Tsai models under the hypothesis that GONSs are randomly or unidirectionally distributed in the cellulose matrix.

3.5. Mechanism for the formation of highly aligned GONSs in the cellulose nanocomposite films

The above results well demonstrated that GONSs could be believed as highly effective enhancers to successfully achieve ultra-low gas permeability and efficient reinforcement of cellulose nanocomposite films, which was no doubt closely related to the horizontal alignment of GONSs, as confirmed by the TEM observation and theoretical simulation results of Cussler and Halpin-Tsai models. Herein, we try to clarify why GONSs are apt to horizontally align the surface of cellulose nanocomposite films. Fig. 11 shows a schematic representation of GONS morphology and its evolution during the fabrication process of the cellulose nanocomposite films. Initially, the strong intra- and inter-molecular hydrogen bonds in cellulose chains are rapidly broken by NaOH at low temperature. Sodium ions, water, and urea molecules form an "overcoat" structure surrounding the cellulose chains to block their self-aggregation, rendering the cellulose chains to be water soluble (Fig. 11a). GONSs are fully exfoliated into individual nanosheets and are randomly dispersed in the NaOH/urea aqueous solvent with the aid of cellulose (Fig. S2, ESI†), arising from the strong interfacial adhesion between GONSs and cellulose chains. In the low-viscosity NaOH/urea aqueous solvent, GONSs are induced by gravitational forces to align parallel to the GCN film surface, owing to the high degree of anisotropy and high aspect ratio of GONSs.[30,60-62] Subsequently, the "overcoat" structure is gradually broken at room temperature to expose the hydroxyl groups of the cellulose, giving rise to the self-association of cellulose chains by hydroxyl junctions (Fig. 11b). As a result, the stable physical cross-linking networks are obtained during the gelation process. And the strong interfacial adhesions between GONSs and cellulose matrix (Figs. 4 and 5) could effectively prevent the GONS aggregation. The interfacial adhesion may have an adverse effect on the orientation of GONSs, however, gravitational forces are probably dominant factors in determining the orientation of GONSs. Finally, the porous cellulose hydrogels are transformed into dense cellulose films and the good alignment of GONSs is further consolidated during the hot pressing (Fig. 11c).[63] Therefore, such a processing procedure results in a typical microstructure with a full exfoliation and high orientation of GONSs in the cellulose matrix, which is beneficial to impart cellulose matrix with ultra-low O_2 permeability and high mechanical performances. The simple, fast, and environmentally friendly processing method opens up a new avenue to fabricate high-performance and multi-functional graphene-based polymer nanocomposites.

Journal of Materials Chemistry A

Cite this: DOI: 10.1039/c0xx00000x

www.rsc.org/xxxxxx

PAPER

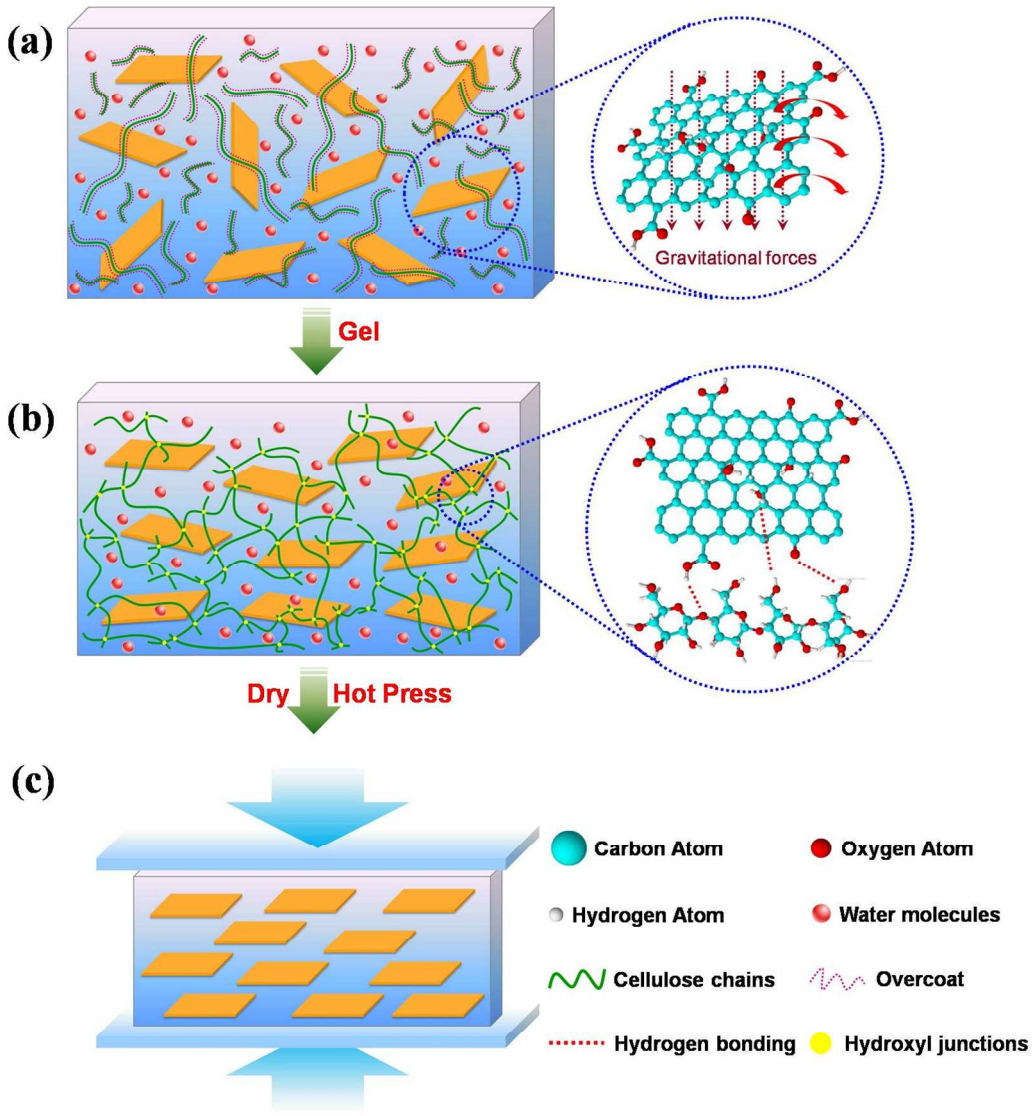

Fig. 11 Schematic representation of GONS morphology and its evolution during the fabrication process of the cellulose nanocomposite films.

4. Conclusions

A simple and environmentally friendly method was proposed to fabricate GONS/regenerated cellulose films using NaOH/urea aqueous solution as the processing solvent. TEM and 2D-WAXD techniques showed that GONSs were fully exfoliated, uniformly dispersed and horizontally aligned along the surface of regenerated cellulose film. Rheological and FTIR measurements also indicated the existence of a large number of strong hydrogen bonding interactions between GONSs and cellulose matrix. A remarkable improvement on barrier properties of the cellulose nanocomposite films was achieved. P_{O_2} was reduced by over three orders of magnitude at a low GONS loading of 1.64 vol%, which was much lower than that of high density polyethylene or poly(ethylene terephthalate), and was comparable to the practical petroleum-based oxygen barrier films such as poly(vinylidene chloride). Moreover, when only adding 1.64 vol% GONSs, the tensile strength and Young's modulus were are enhanced by about 67% and 68% relative to RC film, respectively. The theoretical simulation results of Cussler model and Halpin-Tsai model consistently confirmed that GONSs were apt to align parallel to the film surface. The highly horizontal alignment of GONSs was induced by gravitational forces and was further consolidated by hot pressing in the fabrication of the cellulose nanocomposite films. Given the ultra-low O_2 permeability and high mechanical performance, our cellulose nanocomposite films have excellent potential as packaging materials for protecting

susceptible to O_2 degradation of perishable goods. And the work presented here broadens the application scope of GONSs and promotes the development of both cellulose and GONS-based materials in the packaging and protective industry.

Acknowledgments

The authors gratefully acknowledge the financial support from the National Natural Science Foundation of China (Grant No. 51121001), the Youth Innovation Research Team Special Program of Sichuan Province of China (Grant No. 2013TD0013), the Postdoctoral Science Foundation of China (Grant No. 2012M521691), and the Specialized Research Foundation for the Doctoral Program of High Education (Sichuan University, China) (Grant No. 20120181120101). We are also indebted to the Shanghai Synchrotron Radiation Facility (SSRF, Shanghai, China) for the kind help on 2D-WAXD measurements.

Notes and references

[a] *College of Polymer Science and Engineering, State Key Laboratory of Polymer Materials Engineering, Sichuan University, Chengdu 610065, P. R. China Fax: +86-28-8540-6866; Tel: +86-28-8540-6866; E-mail: ganji.zhong@scu.edu.cn (G.-J. Zhong); zmli@scu.edu.cn (Z.-M. Li)*

[b] *Department of Applied Chemistry, School of Natural and Applied Sciences, Northwestern Polytechnical University, Xi'an 710072, P. R. China*

† Electronic Supplementary Information (ESI) available: Optical image of GONS/cellulose nanocomposite films, Preparation of glycerol toughened cellulose films, the dispersion of GONSs in the preparation process of cellulose nanocomposite films, the crystalline structure of regenerated cellulose, and the summarization of mechanical properties of neat regenerated cellulose and its nanocomposite films incorporated with graphene-based materials. See DOI: 10.1039/b000000x/

1. S. Sinha Ray and M. Bousmina, *Prog. Mater. Sci.*, 2005, **50**, 962-1079.
2. J.-W. Rhim, H.-M. Park and C.-S. Ha, *Prog. Polym. Sci.*, 2013, **38**, 1629-1652.
3. R. A. Gross and B. Kalra, *Science*, 2002, **297**, 803-807.
4. D. Klemm, B. Heublein, H. P. Fink and A. Bohn, *Angew. Chem. Int. Ed.*, 2005, **44**, 3358-3393.
5. R. P. Swatloski, S. K. Spear, J. D. Holbrey and R. D. Rogers, *J. Am. Chem. Soc.*, 2002, **124**, 4974-4975.
6. S. Zhu, Y. Wu, Q. Chen, Z. Yu, C. Wang, S. Jin, Y. Ding and G. Wu, *Green Chem.*, 2006, **8**, 325-327.
7. B. Kosan, C. Michels and F. Meister, *Cellulose*, 2008, **15**, 59-66.
8. H.-P. Fink, P. Weigel, H. Purz and J. Ganster, *Prog. Polym. Sci.*, 2001, **26**, 1473-1524.
9. C. L. McCormick, P. A. Callais and B. H. Hutchinson Jr, *Macromolecules*, 1985, **18**, 2394-2401.
10. A. Striegel, *Carbohyd. Polym.*, 1997, **34**, 267-274.
11. A. Isogai and R. Atalla, *Cellulose*, 1998, **5**, 309-319.
12. R. Gavillon and T. Budtova, *Biomacromolecules*, 2007, **9**, 269-277.
13. Q. Yang, H. Fukuzumi, T. Saito, A. Isogai and L. Zhang, *Biomacromolecules*, 2011, **12**, 2766-2771.
14. H. Qi, J. Liu, S. Gao and E. Mäder, *J.Mater. Chem. A*, 2013, **1**, 2161-2168.
15. E. P. Giannelis, *Adv. Mater.*, 1996, **8**, 29-35.
16. G. Choudalakis and A. Gotsis, *Eur. Polym. J.*, 2009, **45**, 967-984.
17. M. Minelli, M. G. Baschetti and F. Doghieri, *J. Membr. Sci.*, 2009, **327**, 208-215.
18. B. M. Yoo, H. J. Shin, H. W. Yoon and H. B. Park, *J. Appl. Polym. Sci.*, 2014, DOI: 10.1002/app.39628.
19. A. Durmuş, M. Woo, A. Kaşgöz, C. W. Macosko and M. Tsapatsis, *Eur. Polym. J.*, 2007, **43**, 3737-3749.
20. K. Strawhecker and E. Manias, *Chem.Mater.*, 2000, **12**, 2943-2949.
21. N. Tenn, N. Follain, J. Soulestin, R. Cretois, S. Bourbigot and S. Marais, *J. Phys. Chem. C*, 2013, **117**, 12117-12135.
22. P. K. Maji, N. K. Das and A. K. Bhowmick, *Polymer*, 2010, **51**, 1100-1110.
23. T. T. Ho, T. Zimmermann, S. Ohr and W. R. Caseri, *ACS Appl. Mater. Interfaces*, 2012, **4**, 4832-4840.
24. Q. Yang, C.-N. Wu, T. Saito and A. Isogai, *Carbohyd. Polym.*, 2014, **100**, 179-184.
25. H. Kim, Y. Miura and C. W. Macosko, *Chem. Mater.*, 2010, **22**, 3441-3450.
26. S. Morimune, T. Nishino, and T. Goto, *ACS Appl. Mater. Interfaces*, 2012, **4**, 3596-3601.
27. R. Nair, H. Wu, P. Jayaram, I. Grigorieva and A. Geim, *Science*, 2012, **335**, 442-444.
28. Y. H. Yang, L. Bolling, M. A. Priolo and J. C. Grunlan, *Adv. Mater.*, 2013, **25**, 503-508.
29. I. Tseng, Y.-F. Liao, J.-C. Chiang and M.-H. Tsai, *Mater. Chem. Phys.*, 2012, **136**, 247-253.
30. H.-D. Huang, P.-G. Ren, J. Chen, W.-Q. Zhang, X. Ji and Z.-M. Li, *J.Membr. Sci.*, 2012, **409**, 156-163.
31. R. Rajasekar, N. H. Kim, D. Jung, T. Kuila, J. K. Lim, M. J. Park, J. H. Lee, *Compos. Sci. Technol.,* 2013, **89**, 167-174.
32. J.-T. Chen, Y.-J. Fu, Q.-F. An, S.-C. Lo, S.-H. Huang, W.-S. Hung, C.-C. Hu, K.-R. Lee and J.-Y. Lai, *Nanoscale*, 2013, **5**, 9081-9088.
33. S. Morimune, M. Kotera, T. Nishino, T. Goto, *Carbon*, 2014, **70**, 38-45.
34. H.-D. Huang, P.-G. Ren, J.-Z. Xu, L. Xu, G.-J. Zhong, B. S. Hsiao and Z.-M. Li, *J.Membr. Sci.*, 2014, **464**, 110-118.
35. J. Cai and L. Zhang, *Macromol. Biosci.*, 2005, **5**, 539-548.
36. J.-Z. Xu, T. Chen, C.-L. Yang, Z.-M. Li, Y.-M. Mao, B.-Q. Zeng and B. S. Hsiao, *Macromolecules*, 2010, **43**, 5000-5008.
37. B. Duan, C. Chang, B. Ding, J. Cai, M. Xu, S. Feng, J. Ren, X. Shi, Y. Du and L. Zhang, *J.Mater. Chem. A*, 2013, **1**, 1867-1874.
38. J. Liang, Y. Huang, L. Zhang, Y. Wang, Y. Ma, T. Guo and Y. Chen, *Adv. Funct. Mater.*, 2009, **19**, 2297-2302.
39. T. Szabó, O. Berkesi and I. Dékány, *Carbon*, 2005, **43**, 3186-3189.
40. P. Gupta, V. Uniyal and S. Naithani, *Carbohyd. Polym.*, 2013, **94**, 843-849.
41. C.-Y. Liu, G.-J. Zhong, H.-D. Huang and Z.-M. Li, *Cellulose*, 2014, **21**,383-394.
42. J. Cai and L. Zhang, *Biomacromolecules*, 2006, **7**, 183-189.
43. L. Weng, L. Zhang, D. Ruan, L. Shi and J. Xu, *Langmuir*, 2004, **20**, 2086-2093.
44. J. Zhang, Y. Cao, J. Feng and P. Wu, *J.Phys. Chem. C*, 2012, **116**, 8063-8068.
45. C.-J. Kim, W. Khan, D.-H. Kim, K.-S. Cho and S.-Y. Park, *Carbohyd. Polym.*, 2011, **86**, 903-909.
46. D. Han, L. Yan, W. Chen, W. Li and P. Bangal, *Carbohyd. Polym.*, 2011, **83**, 966-972.
47. K. Miller and J. Krochta, *Trends Food Sci. Tech.* 1997, **8**, 228-237.
48. Y. Hu, R. Liu, L. Zhang, M. Rogunova, D. Schiraldi, S. Nazarenko, A. Hiltner and E. Baer, *Macromolecules*, 2002, **35**, 7326-7337.
49. M. Drieskens, R. Peeters, J. Mullens, D. Franco, P. J. Lemstra and D. G. Hristova‐Bogaerds, *J. Polym. Sci.Polym.Phys.*, 2009, **47**, 2247-2258.
50. H. Wang, J. K. Keum, A. Hiltner, E. Baer, B. Freeman, A. Rozanski and A. Galeski, *Science*, 2009, **323**, 757-760.
51. N. K. Lape, E. E. Nuxoll and E. Cussler, *J. Membr. Sci.*, 2004, **236**, 29-37.
52. X. Zhang, X. Liu, W. Zheng and J. Zhu, *Carbohyd. Polym.*, 2012, **88**, 26-30.
53. B. Wang, W. Lou, X. Wang and J. Hao, *J. Mater. Chem.*, 2012, **22**, 12859-12866.
54. S. Mahmoudian, M. U. Wahit, M. Imran, A. Ismail and H. Balakrishnan, *J. Nanosci. Nanotechnol.*, 2012, **12**, 5233-5239.
55. J. Affdl and J. Kardos, *Polym. Eng. Sci.*, 1976, **16**, 344-352.
56. Y. Pan, T. Wu, H. Bao and L. Li, *Carbohyd. Polym.* 2011, **83**, 1908-1915.
57. J. W. Suk, R. D. Piner, J. An and R. S. Ruoff, *ACS Nano*, 2010, **4**, 6557-6564.
58. H.-R. Yang, J. Lei, L. Li, Q. Fu and Z.-M. Li, *Macromolecules*, 2012, **45**, 6600-6610.

59. N. Ning, S. Fu, W. Zhang, F. Chen, K. Wang, H. Deng, Q. Zhang and Q. Fu, *Prog. Polym. Sci.*, 2012, **37**, 1425-1455.
60. S. Ansari, A. Kelarakis, L. Estevez and E. P. Giannelis, *Small*, 2010, **6**, 205-209.
61. S. H. Aboutalebi, M. M. Gudarzi, Q. B. Zheng and J. K. Kim, *Adv. Funct. Mater.*, 2011, **21**, 2978-2988.
62. C. Chen, Q. H. Yang, Y. Yang, W. Lv, Y. Wen, P. X. Hou, M. Wang and H. M. Cheng, *Adv. Mater.*, 2009, **21**, 3007-3011.
63. J. Shang, Y. Zhang, L. Yu, B. Shen, F. Lv and P. K. Chu, *Mater. Chem. Phys.*, 2012, **134**, 867-874.

Graphical Table of Contents

Ultra-low gas permeability and efficient reinforcement of cellulose nanocomposite films by well aligned graphene oxide nanosheets

Hua-Dong Huang,[a] Chun-Yan Liu,[a] Dan Li,[a] Yan-Hui Chen,[b] Gan-Ji Zhong, *[a] Zhong-Ming Li*[a]

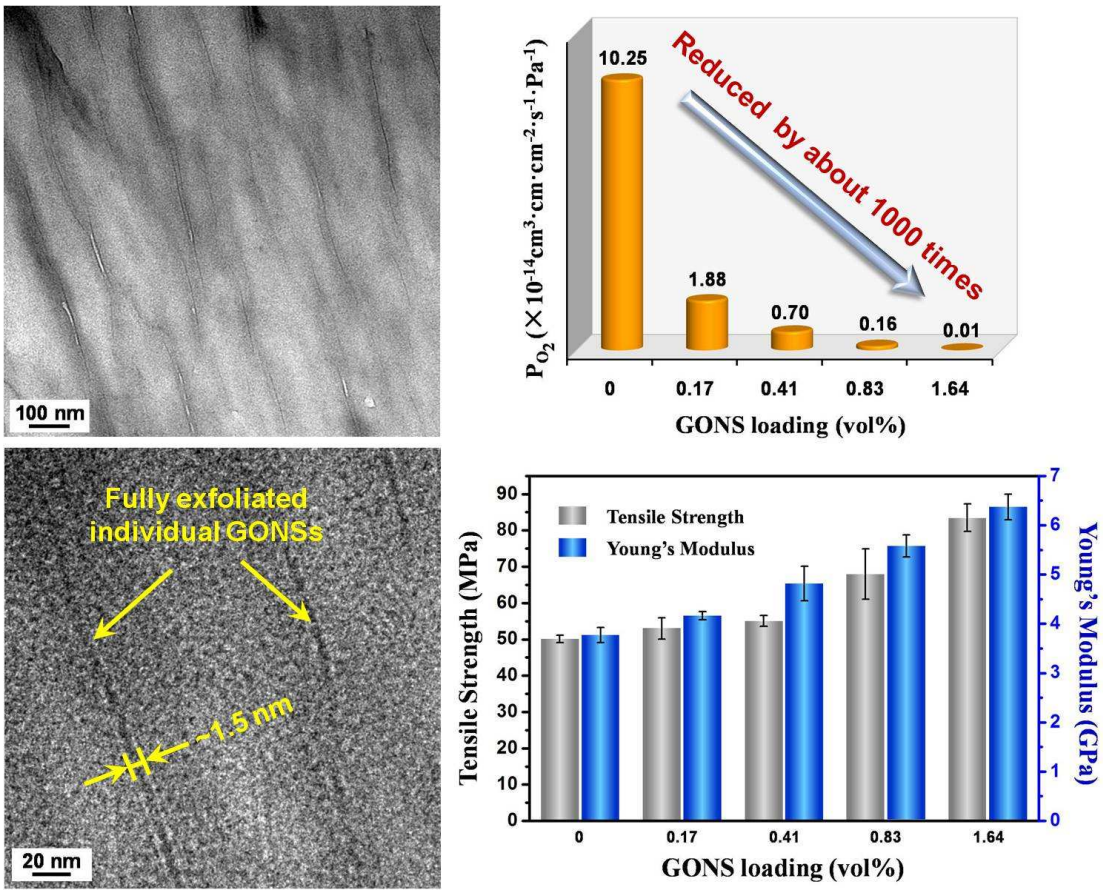

Fully exfoliated and highly aligned GONSs impart regenerated cellulose nanocomposite films with ultra-low O_2 permeability and high mechanical performances.